Journal of
Ship&Ocean
Technology
©JUNE 2008

SOTECH Vol. 12, No. 2, pp. 41 ~ 52, 2008

A Numerical Study on the Flow around a Rudder behind Low Speed Full Ship

Young-Gill Lee[1], Jin-Won Yu[2], Bong-Han Kang[1] and Kyung-Ryeung Pak[2]

[1] Department of Naval Architecture and Ocean Engineering, Inha University, Incheon, Korea
[2] Department of Naval Architecture, Graduate School of Inha University, Incheon, Korea; Corresponding Author: crazyship@inhaian.net

Abstract

The development of a high-lift rudder is needed because low speed full ships such as the VLCC(Very Large Crude oil Carrier) have difficulty for obtaining enough lifting force from a common rudder. The rudder of a ship is generally positioned behind the hull and propeller. Therefore, rudder design should consider the interactions between hull, propeller, and rudder. In the present study, the FLUENT code and body fitted mesh systems generated by the GRIDGEN program are adopted for the numerical simulations of flow characteristics around a rudder that is interacting with hull and propeller. Sliding mesh model(SMM) is adopted to analyze the interaction between propeller rotation and wake flow behind hull. Several numerical simulations are performed to compare the interactions such as hull-rudder, propeller-rudder, and hull-propeller-rudder. Also, we consider relationships between the interactions. The results of present numerical simulations show the variation of flow characteristics by the interaction between hull, propeller, and rudder, and these results are compared with an existing experimental result. The present study demonstrates that numerical simulations can be used effectively in the design of high-lift rudder behind low speed full ship.

Keywords: rudder, lifting force, hull-propeller-Rudder interaction, low speed full ship, numerical simulation

1 Introduction

Of many problems involved in building large vessels, a low speed full ship such as an extra-large oil tanker has difficulty with sufficient control ability because the original rudder may not generate enough lifting force. This problem has caused many marine accidents. In the case of the extra-large oil tankers, even a small accident can lead to severe or long-term damage such as marine pollution. In particular, when low speed is needed such as approaching the entrance to a harbor, passages through narrow waterways, and complicated sea routes, the hull should be assisted by several tugs. Thus, IMO (International Maritime Organization) has reinforced regulations concerning the stability and control of low speed full ships to prevent large marine environmental accidents. Therefore, the necessity in each shipbuilding yard of designing high lifting force rudders

has increased in order to ensure the control ability needed for safe navigation (Lee 2007).

The ability to analyze flow around the rudder is needed to design a high lifting force rudder, and the rudder should be designed in accordance with the analysis results. If fluid flow around the rudder is analyzed using computational fluid dynamics(CFD), the data will increase use of them in designing a rudder. The numerical analysis of flow around a rudder has been used in designs from rudder models with simple forms to rudder models with an extra flap or a gap (Boo et al. 2003, 2004; Choi and Kim 2008; Sarraf et al. 2005). The numerical analysis that considered interactions between the ship hull and propeller was conducted recently by Kong et al. 2002; Kim and Kim 2002; Park et al. 2004, 2007; Boo et al. 2004; Lee et al. 2003; and Simonsen 2000.

The purpose of present study is to visualize the changes of flow characteristics around a rudder caused by ship hull and propeller taking the advantage of numerical methods. We then examine the value of using CFD analysis to design high-lift rudders

2 Numerical computation method

In this research, the body fitted grids are formed using the widely-used GRIDGEN 15.09 program, and numerical values are estimated using the FLUENT 6.3 code. Present research uses several schemes and models as shown in Table 1, which is effective for the computation of NACA0015 as the section of rudder in a turbulent flow model(Standard k-ε model, Sarraf et al. 2005)

Table 1: Numerical schemes for the present numerical simulations of fluid flow

Objects	**Schemes**
Turbulent flow model	Standard k-ε model
Pressure-velocity coupling	SIMPLE (Semi-implicit method for pressure-linked equations)
Differentiation of convection terms	2nd upwind scheme
Propeller rotation	SMM (sliding mesh model)

Two numerical schemes such as MRF(Moving Reference Frame) and SMM are used with FLUENT to represent the revolution of propeller. The MRF scheme calculates a body of rotation by adding a rotational source term to the momentum equation without the revolution of actual grid. This scheme has several advantages in that it can take less computation time and is easily converged relatively. However, the MRF scheme is not suitable when the computation requires the consideration of the wake field, which is not periodically generated from the revolution of propeller or uniform flow field. This is due to the fact that the computations require a condition of steady flow. On the other hand, the SMM scheme calculates the whole grid of the domain by rotating, after dividing the area of the propeller through the user interface. This scheme requires time-marching due to the revolution of propeller. However, it has the advantage that it represents periodicity and can consider the generated wake behind hull.

Given the interaction of wake with hull, the SMM scheme would be suitable for computing the required characteristics with high accuracy in general research such as

present study depending on inflow or the movement of propeller. That is because it is difficult for the MRF scheme alone to obtain satisfying results. The existing studies used the method which has high convergence and which decreases computational time (Park et al. 2004, 2007). This method used the results from steady flow analysis using the MRF scheme as the initial condition. In this research, the SMM scheme is used for the consideration of the interaction between the revolution of propeller and ship hull. Firstly, it is then computed using the MRF scheme, and the results are used as the initial conditions.

3 Objective models and computational conditions

Series60 (C_B=0.8) model, the data for which is easily obtained, is used to model low speed full ships because it is difficult to get real ship data for objective hull forms. The grid is formed from the center of the hull to the stern due to limited computational capacity. The propeller is a fixed four-blade model provided by the part library of AUTOSHIP, and the rudder utilize NACA0015 as the section shape. The rudder stock is left out because of the difficulty of generating grid. The revolution speed of the propeller is established on the basis of a navigation condition of usual VLCC. The principal characteristics of the models used for present computation are shown in Table 2.

Table 2: Principal characteristics of the hull, propeller, and rudder

Hull		Propeller		Rudder	
L_{BP}	5.33m	Blade	4 ea	Section	NACA0015
L/B	6.5	D	0.21 m	Chord	0.102 m
B/T	2.5	J	0.51	Span	0.260 m
C_B	0.8				

The computation is based on a corresponding model speed of the general cruising speed(16 knots) of VLCC(C_B=0.8), and 5 knots to arrive in and depart from the port. This become dimensionless using the Reynolds number, and then is applied to the computation because it neglects the free surface of water. Standard length is based on the chord length of the rudder. The Reynolds number is given by

$$\mathrm{Re} = \frac{\rho u_{\mathrm{inflow}} C}{\mu} \tag{1}$$

where ρ is the density of water, $U_{\mathbf{inflow}}$ is entrance velocity, C is the chord length of the rudder, and μ is the coefficient of viscosity. The Reynolds numbers are estimated to be 4.68 x 10^7 and 1.46 x 10^7, respectively.

The number of propeller revolutions is calculated on the basis of the advance ratio, which is computed to be about 0.51 regardless of Reynolds number. The advance ratio J is given by

$$J = \frac{V}{nD} \tag{2}$$

where V is the advancing velocity of the propeller, n is the number of revolutions, and D is the diameter.

Table 3: Case definition and the number of grids

CASE	Details	Number of grids
CASE 1	Rudder	2.0×10^5
CASE 2	Stern + Rudder	8.0×10^5
CASE 3	Propeller + Rudder	4.0×10^5
CASE 4	Stern + Propeller + Rudder	9.0×10^5

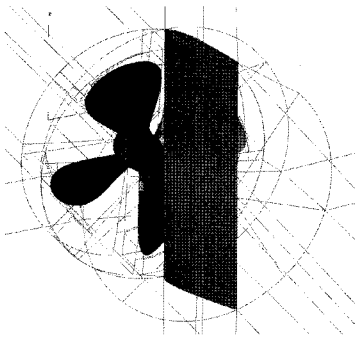

Figure 1: Grid arrangement in CASE 3

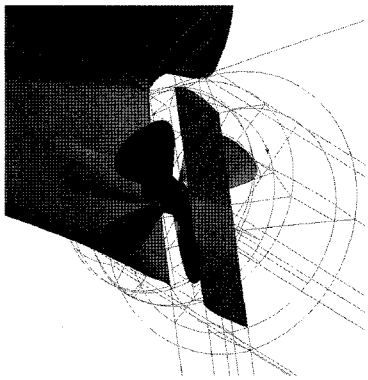

Figure 2: Grid arrangement in CASE 4

A typical steering angle of the rudder is determined to be 20 degrees, at which point separation is expected to begin. Case definitions and the number of grids for each are shown in Table 3. In addition, grid arrangements for CASE 3 and CASE 4 are shown in Figures. 1 and 2.

4 Computational results

In this study, we consider the effect of the hull on the rudder, the effect of the propeller on the rudder, and the influence of the interaction generated from the hull and the propeller on the rudder simultaneously, because we wish to determine the effect of the hull and propeller on the rudder based on computational results from CASE 1 to CASE 4.

The aforementioned four cases are computed at a low speed(5knots) which is simulated for departure and arrival conditions in port, and a high speed(16knots) which is the velocity when the ship is cruising at design speed. Also, the attack angles of the rudder are all 20 degrees, even if it does not fit in with the reality. The lifting force of the rudder is compared after being made dimensionless by C_L. C_L is defined as

$$C_L = \frac{L}{\frac{1}{2}\rho U_{\text{inflow}}^2 A_R} \tag{3}$$

where L is lifting force, ρ is the density of water, U_{inflow} is the entrance velocity, and A_R is the projected square which is obtained by multiplying the span and the length of chord.

Figure 3 shows the limiting streamlines on the rudder surface in CASE 1. As shown in Figure 3, there are few differences in the flow stream over the rudder surface in accordance with the change of Reynolds number. Considering the streamlines of the suction side, separation occurs from the middle of the rudder surface symmetrically. Tip vortices could be discovered at the tip of the rudder, which shows that the decrease of pressure appears at the tip of the rudder. It is thought that the separation phenomenon occur in the middle of the rudder due to a large three-dimensional effect from the tip vortices. The tip vortices are shown in Figure 4 by using the stream-ribbons.

The purpose of CASE 2 is to investigate interactions with the hull and the rudder, and the results of CASE 2 show that the lifting force is lowered.

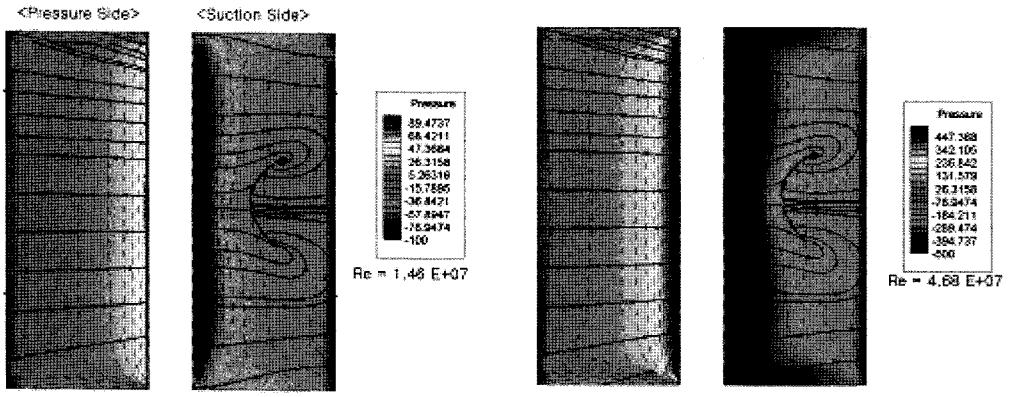

Figure 3: Limiting streamlines and pressure distributions on the rudder surface (CASE 1)

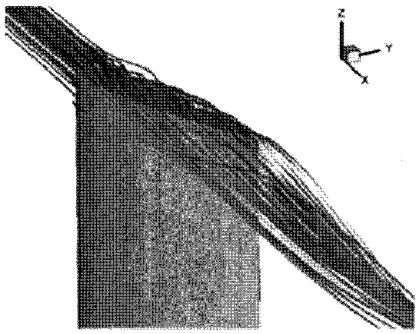

Figure 4: Visualization of rudder-tip vortices with stream-ribbons (CASE 1, Re = 1.46×10^7)

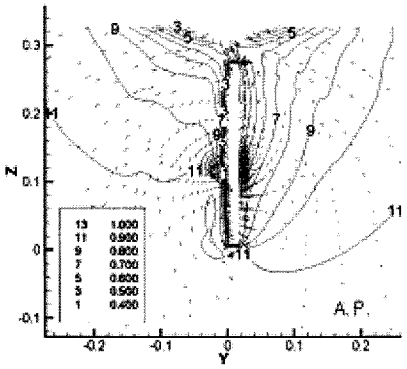

Figure 5: Distribution of axial velocity contours and transverse vectors (CASE 2, Re = 4.68×10^7)

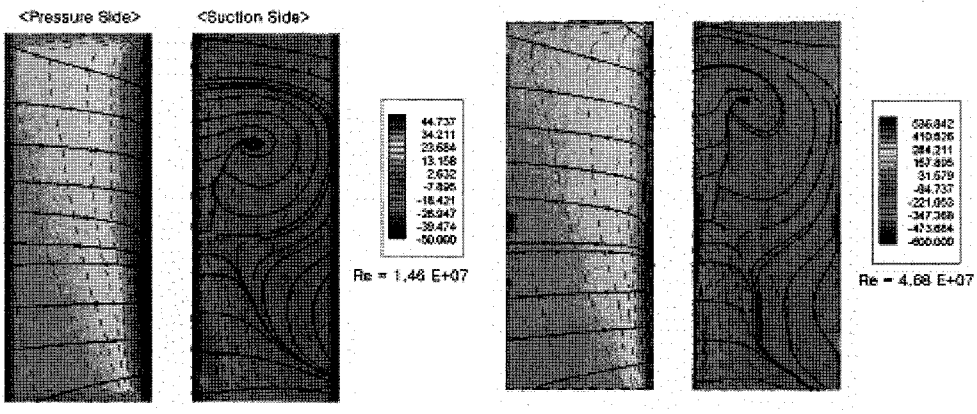

Figure 6: Limiting streamlines and pressure distributions on the rudder surface (CASE 2)

Figure 5 show axial velocity distributions in the direction of the longitudinal axis of ship, and the velocity vectors on the transverse plane at A.P.(After Perpendicular). The length of velocity use dimensionless value using the length of inflow velocity in this study. The rudder is turned to the right in the picture, so the slope of the rudder made the velocity distribution at the right part of the hull widen. In this figure, it is not clear whether or not a bilge vortex occurred, because its computation is only performed about the aft part of ship.

Figure 6 shows pressure on the rudder surface and limiting streamlines in CASE 2. In

this picture, the separation phenomenon is strong, unlike CASE 1; symmetry about the z direction is weakened as well. The pressure on the pressure side of the rudder is increased on the upper side due to the effect of the hull, and the separation point could be seen on the suction side.

CASE 3 is carried out in order to determine the change of flow around the rudder in the wake accelerated by the propeller. The SMM scheme is used to account for the revolution of the propeller. As a result, flow changes around the rudder generated from the revolution of propeller could be seen in Figure 7. This figure shows stream ribbons for Re = 4.68×10^7 to analyze the stream of the entire flow near the rudder for CASE 3. The stream ribbons are abstracted in an arbitrary time. The strong vortices occur at the upper and lower tips of the rudder. Figure 7 is also indicated that the stream ribbons are likely to rotate due to the revolution of the propeller.

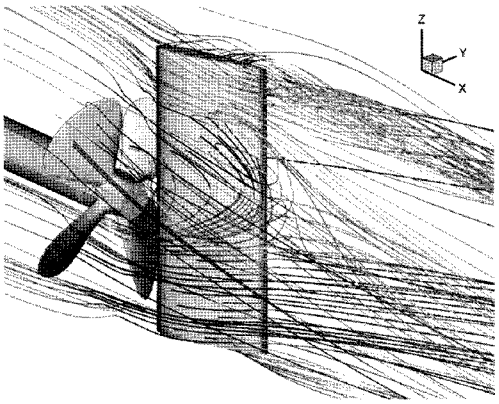

Figure 7: Flow characteristics around the rudder (CASE 3)

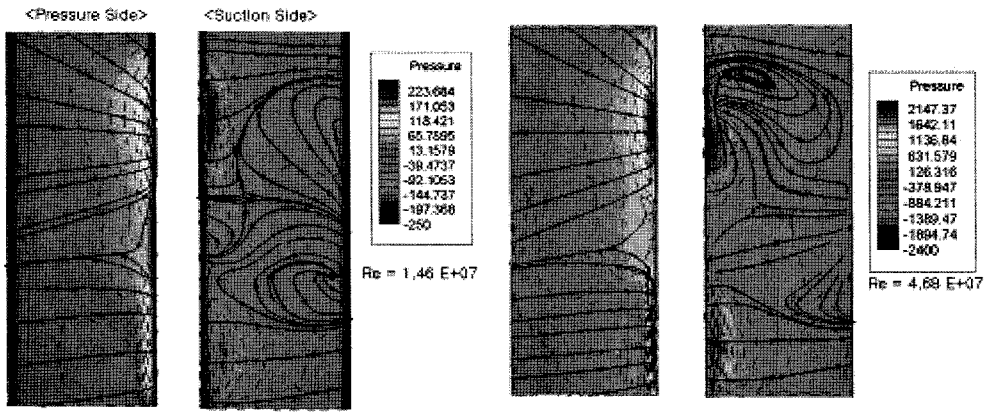

Figure 8: Limiting streamlines and pressure distributions on the rudder surface (CASE 3)

Figure 8 represents the pressure distributions and flow on the limiting rudder surface abstracted at an arbitrary time. In this figure, the high Reynolds number leads to more strong separation, and it can be thought that the increase of the lifting force coefficient in high Reynolds number region is reduced by a strong separation phenomenon. The limiting streamlines are converged on pressure side, because the separation is occurred on the rudder surface of suction side.

Figure 9 shows the change in length of inflow velocity around the rudder as the propeller is rotating. It shows axial velocity distributions in the direction of the

longitudinal axis of ship on the transverse section at A.P., and velocity vectors on this section are accelerated by the propeller. The acceleration does not to be strongly generated from the whole propeller as shown in this picture, but it is mainly occurred from herb to the location of 40~50% in the entire diameter. In addition, it indicates asymmetrical velocity distribution due to the steering angle of the rudder.

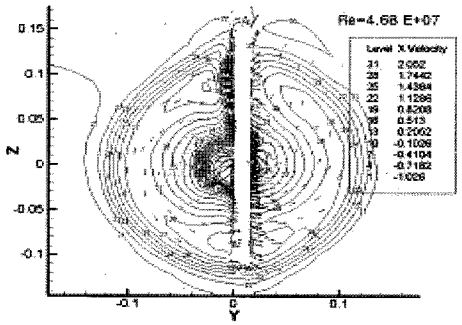

Figure 9: Distribution of axial velocity contours and transverse vectors at A.P. (CASE 3, Re = 4.68 x10^7)

In CASE 4, the interaction phenomenon between the hull, propeller, and rudder are computed. In this case, additional interaction with the hull and the propeller, as well as the interaction with hull-rudder and propeller-rudder, could be considered by comparing the coefficient values of the lifting force, as previously mentioned.

Figure 10 shows the pressure distributions and flow over the rudder surface in CASE 4. The limiting streamlines on the rudder surface comes into view in a radial shape on the pressure side of the rudder as shown in Figure 10, because the accelerating flow influenced by the propeller conflicts with the rudder. Figure 11 shows the flow characteristics around the rudder in CASE 4. This figure shows that the flow are accelerated and revolved due to the effect of the hull and the propeller.

Figure 12 show axial velocity distributions in the direction of the longitudinal axis of ship and the vectors on the transverse planes to determine what the propeller, the hull, and the rudder affect. This figure shows that severe revolution on the suction side expected strong separation, as compared with Figure 10.

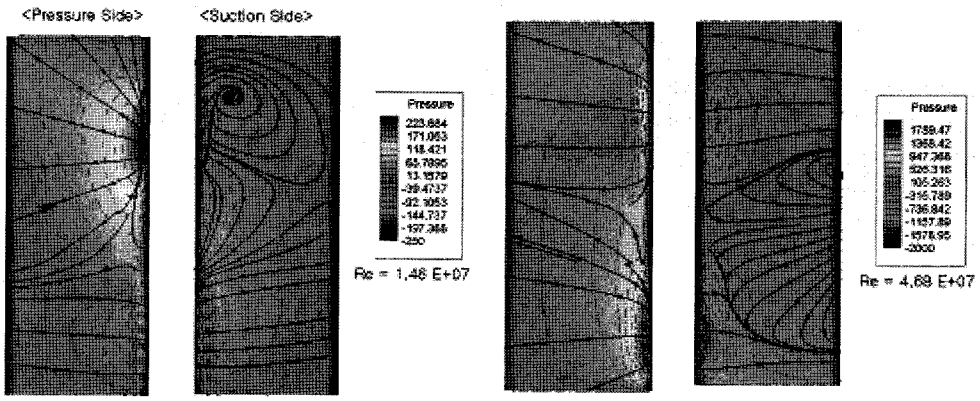

Figure 10: Limiting streamlines and pressure distributions on the rudder surface (CASE 4)

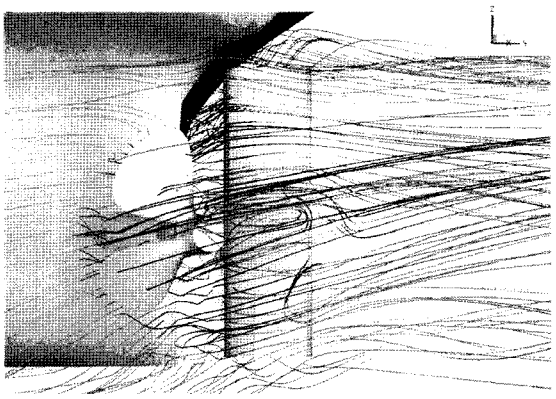

Figure 11: Flow characteristics around the rudder (CASE 4, Re = 4.68 x10^7)

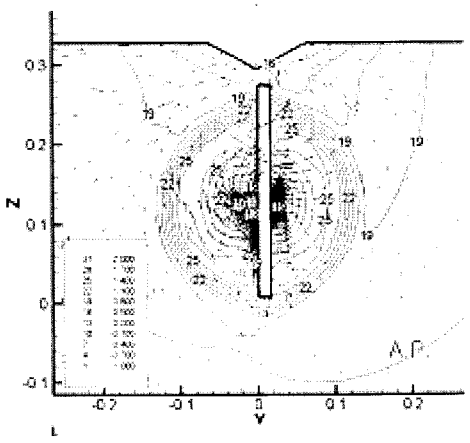

Figure 12: Distribution of axial velocity contours and transverse vectors (Re = 4.68 x10^7).

Table 4: Comparison of lift coefficients

Re	CASE	C_L	Dis. C_L	Dis. %
1.46x10^7	CASE1	0.855	-	-
	CASE2	0.600	-0.255	-29.8
	CASE3	1.896	+1.041	+121.8
	CASE4	1.310	+0.455	+53.2
4.68x10^7	CASE1	0.854	-	-
	CASE2	0.502	-0.352	-41.2
	CASE3	1.781	+0.927	+108.5
	CASE4	1.350	+0.496	+58.0

Table 4 compares the coefficient of lifting force (C_L) that is obtained through the present numerical simulation with each CASE. Dis. means the changed ratio of the coefficient of lifting force which is based on the computations performed only for the rudder (CASE 1), and Dis. % is the ratio.

There are few changes in accordance with the difference of Reynolds numbers in CASE 1, as compared to the coefficient value of lifting force computed. However, there are a few differences in the coefficient values of the lifting force in CASE 2, CASE 3, and CASE 4. In addition, the changed ratio of the coefficient of lifting force in CASE 4 can't be predicted with the changed ratio of the coefficient of lifting force in CASE 2 and CASE 3. This means that additional interaction between the hull and the propeller has occurred.

Also, experimental data based on papers describing experiments on a section of rudder, NACA0020, using four blades, advance ratio (J)=0.51, and the angle of attack=20 degrees (Turnok and Molland 2000, Molland and Turnok 2002), is shown in Table 5, similar to the data in Table 4. This experiment used a wind tunnel test and some different models as compared with the present study. However, it will be reasonable to use this data to help understand the overall trend.

Table 5: Comparison of lift coefficients (Molland's Experiment)

CASE	C_L	Dis.C_L	Dis.%
CASE1	0.92	-	-
CASE2	-	-	-
CASE3	1.7	+0.78	+84.8
CASE4	1.40	+0.48	+52.2

The rudder cross-section, blade shape, and Reynolds number are some different in comparing Table 4 with Table 5, but the computational results about the variation of lift coefficient are qualitatively similar each other in each CASE.

Figure 13 shows the change of lifting force in CASE 1 and CASE 4 in accordance with the attack angle of the rudder. As shown in this figure, the increased values of the coefficient of lifting force in CASE 1 and CASE 4 in accordance with increasing the attack angle are different. The coefficient of lifting force in CASE 4 is larger than that in CASE 1. When the angle of attack is 20 degrees, the difference is about 58% based on the lift coefficient in CASE 1. This means that the direct access needs because it is difficult to predict the performance of rudder device in case that it is placed at the wake of hull and propeller.

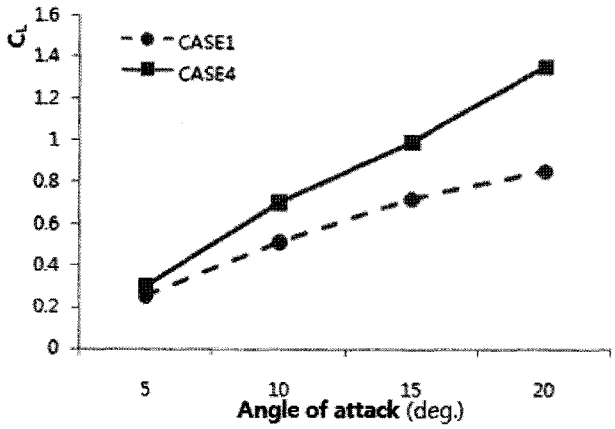

Figure 13: Comparison of lift coefficients between CASE 1 and CASE 4 (Re = 4.68 x10^7).

5 Conclusions

This study is performed in order to numerically determine the flow characteristics and pressure distributions around the rudder device in case that it is placed at the wake of propeller and hull about a low speed full ship. Several computations are carried out to find out how the stern or propeller affects the rudder for the cases of hull-rudder, propeller-rudder, and hull-propeller-rudder interactions. Then, the results of each case are compared.

1) The computational results show that interaction with hull-rudder, propeller-rudder and hull-propeller influences the pressure distribution on the rudder and the surrounding flow field.
2) It is known that the direct access to interaction with hull-propeller-rudder needs, because it is difficult to predict interaction with hull-propeller-rudder through interaction with hull-rudder, propeller-rudder.
3) The changed ratio of the coefficient of lifting force along the interaction with the hull-propeller-rudder is almost the same between the experimental results and computational results. Therefore, numerical computations could confirm that changes in pressure characteristics and flow around the rudder with the effects of hull and propeller wake. Also, the variation of lifting force could be predicted.
4) We believe that if future numerical simulations are conducted carefully by focusing on practical models, then numerical simulation will be effective in designing rudder such as a high lifting force rudder for a low speed full ship.

Acknowledgements

This work was supported by a Korea Science and Engineering Foundation(KOSEF) grant funded by the Korean government(MEST) (No. ROA-2007-000-10028-0).

References

Boo, K.T., Y.H. Ji, Y.S. Kim and S.C. Shin. 2004. A Numerical Study of Hydrodynamic Forces Acting on Rudders. Journal of the Society of Naval Architects of Korea, **41**, **2**, 61-69.

Boo, K.T., C.B. Hong and K.J. Lee. 2004. Simulation of viscous flow around the ship appended with the propeller and the rudder. Proceedings of the Annual Autumn Meeting The Society of Naval Architects of Korea, Sancheong, 527-531.

Choi, J.E. and J.H. Kim. 2008. FLOW CHARACTERISTICS AROUND A RUDDER IN OPEN LATER CONDITION, Journal of computational fluids engineering, **13**, **1**, 14-20.

Kim, D.S. and H.T. Kim. 2002. Analysis of Open-Water Characteristics of Marine Propeller by Computational Method for Viscous Flow. Journal of the Society of Naval Architects of Korea, **39**, **3**, 8-17.

Kong, D.-S., J.-M. Han and J.-M. Lew. 2002. A Study on the Pressure Distributions of Horn Rudder Operating in Ship's Wake. Journal of the Society of Naval Architects of Korea, **39**, **2**, 1-10.

Lee, H.S., S.A. Kinnas, H. Gu and S. Natarajan. 2003. Numerical modeling of rudder sheet cavitation including propeller/rudder interaction and the effects of a tunnel. Fifth International Symposium on Cavitation(CAV2003).

Lee, S.H. 2007. Marine High Lifting Rudder Device and a Development of Application Technology. Report No. ROA-2007-000-10028-0, Ministry of Science and Technology, South Korea.

Molland, A.F. and S.R. Turnock. 2002. FLOW STRAIGHTENING EFFECTS ON A SHIP RUDDER DUE TO UPSTREAM PROPELLER AND HULL. Int. Shipbuild. Progr., **49**, **3**, 195-214.

Park, J.-J, Y.-B. Choi and Y.-S. Hwang. 2004. A Study on the characteristics of viscous flows around a Hull by Propeller effect. Proceedings of the Annual Autumn Meeting The Society of Naval Architects of Korea, Sancheong, 583-588.

Park, J.-J., Y.-H. Jang and Y.-B. Choi. 2007. A CFD analysis on the rudder design considering the hull and propeller rotation. Proceedings of the Annual Autumn Meeting The Society of Naval Architects of Korea, Jeju, 1183-1188.

Sarraf, C., R. Jaouen, H. Djeridi and J.Y. Billard. 2005. Investugation of thickness effects on 2D NACA symmetric foils. IEEE, 1298-1303.

Simonsen, C.D. 2000. Rudder, Propeller and Hull interaction by RANS. Department of Naval Architecture & Offshore Engineering Technical University of Denmark.

Turnock, S.R. and A.F. Molland. 2000. Directly coupled fluid structural model of a ship rudder behind a propeller, Marine Structures 13 (2000). 53-72.